

FEATURE SELECTION IN HIGH-DIMENSIONAL SPACES USING GRAPH-BASED METHODS

SWARNADIP GHOSH, SOMABHA MUKHERJEE, DIVYANSH AGARWAL, YICHEN HE,
MINGZHI SONG, AND XUEJIAO PEI

ABSTRACT. High-dimensional feature selection is a central problem in a variety of application domains such as machine learning, image analysis, and genomics. In this paper, we propose graph-based tests as a useful basis for feature selection. We describe an algorithm for selecting informative features in high-dimensional data, where each observation comes from one of K different distributions. Our algorithm can be applied in a completely nonparametric setup without any distributional assumptions on the data, and it aims at outputting those features in the data, that contribute the most to the overall distributional variation. At the heart of our method is the recursive application of distribution-free graph-based tests on subsets of the feature set, located at different depths of a hierarchical clustering tree constructed from the data. Our algorithm recovers all truly contributing features with high probability, while ensuring optimal control on false-discovery. We show the superior performance of our method over other existing ones through synthetic data, and demonstrate the utility of this method on several real-life datasets from the domains of climate change and biology, wherein our algorithm is not only able to detect known features expected to be associated with the underlying process, but also discovers novel targets that can be subsequently studied.

1. INTRODUCTION

High dimensional statistical problems arise frequently across diverse fields of scientific research. Variable selection plays a pivotal role in such settings. For example, with an estimated 30,000 genes in the human genome, computational investigations in genomics often seek to identify the features of utmost importance, either to a disease, developmental or physiological process. In such high-dimensional data analyses, robust and scalable methods for feature selection are of paramount importance [16]. Several methods have been developed for high dimensional linear regression such as the lasso(see [19]). The quality of a feature selection mechanism is often compromised under model misspecifications by the high-dimensional nature of the data. When there are a large number of nuisance parameters in a misspecified model, parametric methods such as regression often perform poorly, especially so in high-dimensional setups. This necessitates the development of non-parametric methods, which make no distributional assumptions on the data, but are still powerful for a wide class of alternatives.

In this paper, we are interested in the problem of variable selection in the following distributional context. Suppose we have data coming from several multivariate

Key words and phrases. graph-based tests, hierarchical correlation clustering.
The first two authors contributed equally to the paper.

distributions, and we want to detect any non homogeneity across these distributions. In Statistics, this scenario is addressed by the classical K sample problem where one concludes that K multivariate distributions are non-identical based on some test statistics. Our target is to understand which marginals of these multivariate distributions contribute the most to their overall change, if any.

Understanding the important variables for a K sample problem that cause a distributional difference is of practical importance as it can provide actionable features for further investigation. For univariate data, there are several celebrated distribution-free two-sample tests such as the Kolmogorov-Smirnov maximum deviation test [18], the Wald-Wolfowitz runs test [20], and the Mann-Whitney rank-sum test [9] (see [5] for more on these tests). In the multivariate scenario, distributional variations in the dataset are often amplified by the joint effects of some closely related features, rather than individual effects examined in isolation. The multivariate dependency structure motivated researchers to generalize univariate methods to higher dimensions (See [21, 1]). Friedman and Rafsky [3] proposed a multivariate two-sample test (multivariate run test) to test homogeneity based on the minimal spanning tree¹ of the sample points, and Schilling [22] proposed a multivariate two-sample test based on the nearest neighbor graph. Even though many of these methods can be effectively used in high-dimensional problems, none of them inherit the exact distribution-free property of the univariate tests. Biswas et al. [2] proposed another two-sample test based on Hamiltonian cycles, which is distribution-free in finite samples. However, computing the minimum weight Hamiltonian path is NP-hard, making this test computationally prohibitive beyond small sample sizes.

In this work we use the exact distribution free multisample test developed in [14], a generalization of the multivariate two-sample *crossmatch test* introduced by Rosenbaum [15], to test homogeneity across multiple samples. This test is based on the number of between-sample edges in the minimum non-bipartite matching graph constructed on the pooled sample. This method is computationally efficient since the test statistic can be computed in time which is polynomial in both the number of samples and the dimension of the data. We perform the test in a hierarchical way with a stopping rule based on adjusted p value to identify the important set of variables in this K sample framework. For this purpose, we use the hierarchical clustering approach proposed in [12]. This method begins by testing distributional homogeneity across all the variables. Depending on whether there is enough evidence of non-homogeneity, the method then proceeds by testing homogeneity across smaller subsets of variables and may continue till individual variables are reached. The smallest possible sets of variables, which still exhibit a significant evidence of distributional difference, are retained. The final outcome of this method is a subset of variables, which are minimally significant, i.e., do not contain redundant non-significant variables. Since this method is based on graph-based multisample tests, we call it the *graph-based feature selection* (GFS) algorithm. With increasing sample size, the proportion of true signals recovered by the GFS algorithm

¹Given a finite set $S \subset \mathbb{R}^d$, the *minimum spanning tree* (MST) of S is a tree with vertex-set S , which has the minimum value of sum of the Euclidean lengths of its edges.

approaches 1, while at the same time ensuring a control on the probability of discovering at least one false signal.

The rest of the paper is organized as follows. We begin by describing the GFS algorithm in Section 2. Section 3 gives theoretical guarantees of our algorithm. In section 4, we provide numerical experiments under a variety of setups with varying location and scale parameters, and demonstrate the efficacy of the GFS in such cases. The procedure is then applied on a forest fires data, a single cell transcriptomics data, a mice protein data, and a brain cancer data in Section 5. Section 6 concludes the paper with a discussion. Finally, the Appendix provides proofs of the lemmas quoted in the main body of the manuscript.

2. METHODOLOGY

In this section, we describe our graph-based feature selection (GFS) algorithm. Suppose that we have K unknown multivariate probability distributions F_1, \dots, F_K on \mathbb{R}^d . For each $1 \leq i \leq K$, suppose that we have access to n_i observations from the distribution F_i . We assume that all the $n := n_1 + \dots + n_K$ observations are independent. Our goal is to select those marginals of F_1, \dots, F_K , which contribute the most to the difference in these distributions, if there is any.

The n observations are stacked along the rows of an $n \times d$ data matrix \mathbf{X} , with the first n_1 rows of \mathbf{X} denoting the observations coming from F_1 , the next n_2 rows of \mathbf{X} denoting the observations coming from F_2 , and so on. For a set $S \subseteq [d] := \{1, \dots, d\}$, let \mathbf{X}_S denote the submatrix of \mathbf{X} formed by all the rows of \mathbf{X} and only those columns of \mathbf{X} whose indices are in S . Hence, \mathbf{X}_S is an $n \times |S|$ matrix. Suppose that we have a non-parametric test T that can test

$$H_0 : F_1 = \dots = F_K \quad \text{v.s.} \quad H_1 : F_i \neq F_j \text{ for some } 1 \leq i < j \leq K$$

based on a data matrix of observations from F_1, \dots, F_K . A natural choice of T is any non-parametric distribution-free graph-based test for equality of multivariate distributions (for example, the MCM and the MMCM tests in [14]).

The algorithm starts by constructing a tree \mathcal{T} of clusters, satisfying the following properties:

- (1) The root node of \mathcal{T} is the set $[d]$.
- (2) Every non-leaf node C of \mathcal{T} has two children, which are disjoint sets uniting to C .
- (3) The leaf nodes of \mathcal{T} are singleton sets.

The hierarchical structure of \mathcal{T} implies that for any two nodes C and D of \mathcal{T} , either $C \subseteq D$ or $D \subseteq C$ or $C \cap D = \emptyset$.

A natural way to construct such a tree \mathcal{T} is to use a hierarchical clustering procedure like Single Linkage agglomerative clustering (see [6], [10], [11]). Some other hierarchical clustering methods can be found in [13], [4]. The starting point of this procedure is a matrix $D \in \mathbb{R}^{d \times d}$ of pairwise dissimilarities between the variables $1, \dots, d$. In the simulation and real data analysis parts of this paper, we take $D = J - R$, where R is the correlation matrix of the d variables and J is the matrix of all ones. The tree is built in a sequential way. In the beginning of the agglomerative clustering process,

each element is in a cluster of its own. The clusters are then sequentially combined into larger clusters, until all elements end up being in the same cluster. At each step, the two clusters separated by the shortest distance are combined. For Single Linkage agglomerative clustering, the distance between two clusters is defined as the minimum distance between elements of the two clusters.

Once the tree \mathcal{T} is constructed, the next step is to get hold of some *minimally significant* subsets of features. Towards this, we need a couple of definitions.

Definition 1. *The adjusted p-value of a node C in the tree \mathcal{T} is defined as:*

$$p_{\text{adj}}^C := p^C \frac{d}{|C|},$$

where $|C|$ denotes the cardinality of C , and p^C denotes the p-value of the test T conducted on the matrix \mathbf{X}_C .

Definition 2. *For $\alpha \in [0, 1]$, a node C in the tree \mathcal{T} will be called an α -terminal node, if the following three conditions are satisfied*

- (1) $p_{\text{adj}}^C \leq \alpha$;
- (2) $p_{\text{adj}}^B \leq \alpha$ for every ancestor B of C in the tree \mathcal{T} ;
- (3) $p_{\text{adj}}^B > \alpha$ for every child B of C in the tree \mathcal{T} .

Note that condition (2) in Definition 2 is satisfied vacuously by the root node of \mathcal{T} , and condition (3) is satisfied vacuously by the leaf nodes of \mathcal{T} . Our final set of selected features at level α , is the union of all the α -terminal nodes of \mathcal{T} . Below, we give an algorithmic implementation of our feature selection procedure.

Algorithm 1: Feature Selection Algorithm

Input: A tree \mathcal{T} satisfying (1), (2) and (3)

Output: A set $S \subseteq [d]$ of selected variables

- 1 **Initialization:** Set C to be the root node of \mathcal{T} and $S = \emptyset$;
 - 2 Perform the test T on \mathbf{X}_C and report the adjusted p-value p_{adj}^C . If $p_{\text{adj}}^C > \alpha$ and $C = [d] := \{1, 2, \dots, d\}$, stop the algorithm; else if $p_{\text{adj}}^C \leq \alpha$ and $|C| = 1$, set $S \leftarrow S \cup C$; else if $p_{\text{adj}}^C \leq \alpha$ and $\min\{p_{\text{adj}}^{C_1}, p_{\text{adj}}^{C_2}\} > \alpha$ for children C_1, C_2 of C , set $S \leftarrow S \cup C$; else go to Step 3;
 - 3 Perform Step 2 with C replaced by every child B of C satisfying $p_{\text{adj}}^B \leq \alpha$.
-

Algorithm 1 is implemented as a binary recursion in the R package GFS (under preparation).

3. THEORETICAL GUARANTEES OF THE GFS ALGORITHM

In this section, we prove some theoretical guarantees of the GFS algorithm. In order to do so, we need to define a precise notional framework for features/marginals of multivariate distributions that contribute to their difference. To start with, the null hypothesis for a set of features $L \subseteq [d]$ is defined as:

$$H_{0,L} : F_{1[L]} = \dots = F_{K[L]}$$

where $F_{i[L]}$ denotes the joint distribution of $(X_j)_{j \in L}$ where $X := (X_1, \dots, X_d) \sim F_i$. We call a set of features $L \subseteq [d]$ a *signal set*, if:

- (1) H_{0,L^c} is true.
- (2) $\forall L' \subseteq L$, $H_{0,L'}$ is not true.

It follows from Lemma 1 that a signal set is unique. We can now define the family-wise error rate (FWER), false discovery rate (FDR) and power of a feature selection procedure.

Definition 3. Let L be the signal set. The FWER, FDR and power of a feature selection procedure reporting a (random) set of selected features S are defined as:

- (1) $\text{FWER} := \mathbb{P}(S \setminus L \neq \emptyset)$;
- (2) $\text{FDR} := \mathbb{E}(|S \setminus L| / \max\{|S|, 1\})$;
- (3) $\text{Power} := \mathbb{P}(L \subseteq S)$.

Theorem 1. Suppose that d is fixed as $n \rightarrow \infty$. Then, in the asymptotic regime where the underlying test T is consistent at every level, the power of the GFS algorithm goes to 1, whereas the FWER and FDR is controlled at level $\alpha + o(1)$.

Proof. Let L be the signal set and S be the set of selected features. We start by showing that the power of the GFS algorithm goes to 1. Towards this, note that for every set B containing some $\ell \in L$, $H_{0,B}$ is not true, and hence, by the consistency of the test T at every level, we have:

$$\mathbb{P}(p_{\text{adj}}^B \leq \beta) \rightarrow 1 \quad \text{for all } \beta > 0$$

which is same as saying that $p_{\text{adj}}^B \rightarrow 0$ in probability. Since d is fixed, we have:

$$\max\{p_{\text{adj}}^B : \ell \in B \text{ for some } \ell \in L\} \rightarrow 0 \quad \text{in probability.} \quad (1)$$

It follows from (1) that

$$\max\{p_{\text{adj}}^B : B = \{\ell\} \text{ or } B \text{ is an ancestor of } \{\ell\} \text{ in } \mathcal{T} \text{ for some } \ell \in L\} \rightarrow 0 \quad \text{in probability.}$$

This shows that

$$\mathbb{P}(\text{every } \{\ell\} \subseteq L \text{ is an } \alpha\text{-terminal node}) \rightarrow 1. \quad (2)$$

Since S was defined as the union of all α -terminal nodes, it follows from (2) that $\mathbb{P}(L \subseteq S) \rightarrow 1$, i.e. the power of the GFS algorithm goes to 1.

Next, we show that the FWER of the GFS algorithm is $\alpha + o(1)$. Towards this, suppose that $S \setminus L \neq \emptyset$, and choose $v \in S \setminus L$. Since $v \in S$, $v \in V$ for some α -terminal node V of \mathcal{T} . Now, there may be two cases. If $V \subseteq L^c$, then by (1), $H_{0,V}$ is true. Also, since V is an α -terminal node,

$$\max_{U \in \mathcal{T}: U \supseteq V} p_{\text{adj}}^U \leq \alpha.$$

Hence, $V \in \mathcal{T}_0 \cap \mathcal{T}_{\text{rej}}$, where \mathcal{T}_0 and \mathcal{T}_{rej} are defined in the statement of Lemma 2. This implies that $\mathcal{T}_0 \cap \mathcal{T}_{\text{rej}} \neq \emptyset$. Otherwise, V contains some $\ell \in L$. Thus, $|V| \geq 2$, and hence, V has two non-empty children V_1 and V_2 . By (2), $\ell \in V_i$ for some $i \in \{1, 2\}$. By

(2) $H_{0,\{\ell\}}$ is not true, and hence, H_{0,V_i} is not true. Also, since V is an α -terminal node, $p_{\text{adj}}^{V_i} > \alpha$. Hence, we have:

$$\{S \setminus L \neq \emptyset\} \subseteq \{\mathcal{T}_0 \cap \mathcal{T}_{\text{rej}} \neq \emptyset\} \bigcup \bigcup_{\substack{V \subseteq [d]: H_{0,V} \\ \text{is not true}}} \{p_{\text{adj}}^V > \alpha\}.$$

By Lemma 2, $\mathbb{P}(\mathcal{T}_0 \cap \mathcal{T}_{\text{rej}} \neq \emptyset) \leq \alpha$. Also, by consistency of T , we know that $\mathbb{P}(p_{\text{adj}}^V > \alpha) = o(1)$ for all $V \subseteq [d]$ such that $H_{0,V}$ is not true. Since d is fixed, it follows that $\mathbb{P}(S \setminus L \neq \emptyset) \leq \alpha + o(1)$. The FDR control at level α follows from the fact that $FDR \leq FWER$. This completes the proof of Theorem 1. \square

4. SIMULATIONS

In this section, we show the performance of our feature selection algorithm when the test T is the MMCM test (see [14]), and the underlying distributions are assumed to be taken from a location and a scale family. The MMCM test starts by constructing a vector $\mathbf{A} := ((A_{ij}))_{1 \leq i < j \leq K}$ of cross-counts, where A_{ij} denotes the number of edges in the minimal non-bipartite matching graph² constructed on the n sample points, that have one endpoint coming from F_i and the other endpoint from F_j . It was shown in [14] that the vector \mathbf{A} is distribution free under the null hypothesis of distributional equality. Using this fact, the MMCM test statistic is defined as:

$$T := (\mathbf{A} - \mathbb{E}_{H_0} \mathbf{A})^\top \text{Cov}_{H_0}^{-1}(\mathbf{A})(\mathbf{A} - \mathbb{E}_{H_0} \mathbf{A})$$

where \mathbb{E}_{H_0} and Cov_{H_0} denote the expectation and covariance operators under the null hypothesis of distributional equality. The null hypothesis is rejected for large values of T . Although this test is distribution-free under the null, its asymptotic $\chi_{\binom{K}{2}}^2$ distribution is often more useful in practice for choosing the exact rejection threshold.

Each of the location and scale settings is executed in the distributional framework when the underlying data is generated from a multivariate normal distribution. A typical case looks as follows. The d -variate normal distributions are perturbed in randomly chosen s marginals j_1, j_2, \dots, j_s , and the remaining $d - s$ marginals are taken to be standard Gaussians. In the location setting, the perturbations in the s marginals are in the means, with variances fixed at 1, while in the scale setting, the perturbations in the s marginals are in the variances, with means fixed at 0. In each setting, we run R replications of this experiment, resulting in R -many tuples of selected variables. We then report the empirical versions of the FWER, FDR and **power of the GFS algorithm conducted at 5% level, over the R replications.** This means probability that rejecting null hypothesis given alt is true is 5% over R replications

4.1. The Location Setting: In this setting, we start with a fixed vector $\boldsymbol{\mu}$ of length d . We then randomly choose s -many entries of $\boldsymbol{\mu}$ and make them all equal to some θ . The remaining entries of $\boldsymbol{\mu}$ are set at 0. The distribution F_i is then taken to be the multivariate Gaussian with mean $i\boldsymbol{\mu}$ and identity covariance matrix for $1 \leq i \leq K$. We vary θ in the set $\{0.15, 0.2, \dots, 0.70, 0.75\}$ and take $d = 100$, $s = 25$, $R = 100$. We

²The minimal non-bipartite matching graph on n nodes is defined as a matching on these n points that has minimum value of the sum of Euclidean lengths of edges. d dimensions, s marginals (features) and R replications

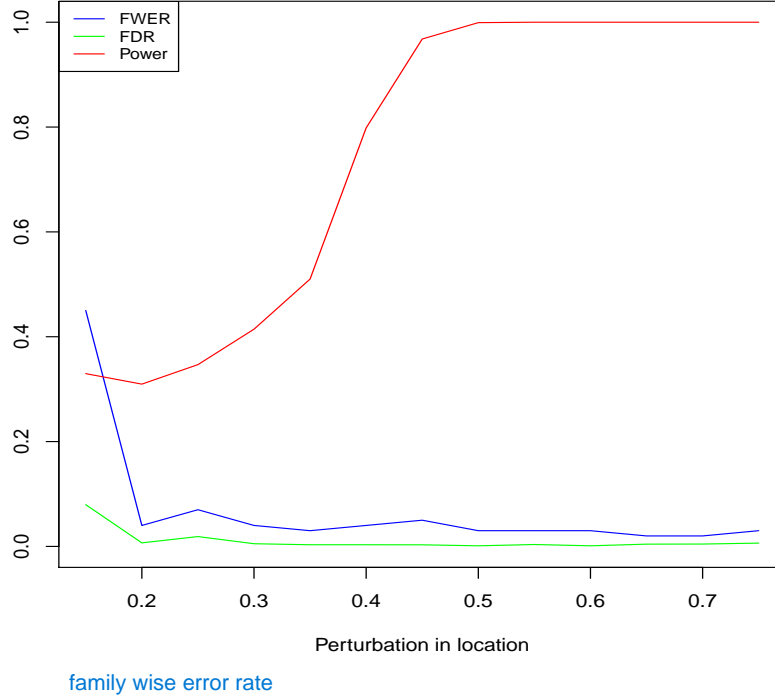


FIGURE 1. **FWER**, **FDR** and power of the GFS algorithm using the MMCM test in the location setting

False Discovery rate = false positives/total positives

set the number of classes $K = 5$, with all class sizes = 200, and report the empirical FWER, FDR and power over R replications. The graphs of the empirical FWER, FDR and power are given below, and the exact numerics are presented in Appendix 8.2.

4.2. The Scale Setting: In this setting, we start with a fixed positive real number θ . We then randomly choose s -many indices from $\{1, \dots, d\}$, and define F_i as a d -variate normal distribution with mean zero, and covariance matrix obtained by replacing the s many chosen diagonal entries of the identity matrix, by $1 + (i - 1)\theta$. We vary θ in the set $\{1, 1.5, 2, 2.5, \dots, 14, 14.5, 15\}$ and take $d = 100$, $s = 25$, $R = 100$. We set the number of classes $K = 5$, with class sizes = 200.

Figures 1 and 2 show that the (empirical) power of the GFS algorithm increases to 1 as the perturbation in location/scale increases, whereas the FDR and FWER decrease sharply, and fall below the 5% level with increase in perturbation.

Basically perturbations in scale and location make GFS more powerful

4.3. Comparison with the Kruskal Wallis test in location-scale family with dependence: For this simulation we consider a similar set up as before. We take F_i to be a d -variate normal distribution with mean $\mu^{(i)}$ and covariance matrix $\Sigma^{(i)}$ of the following form:

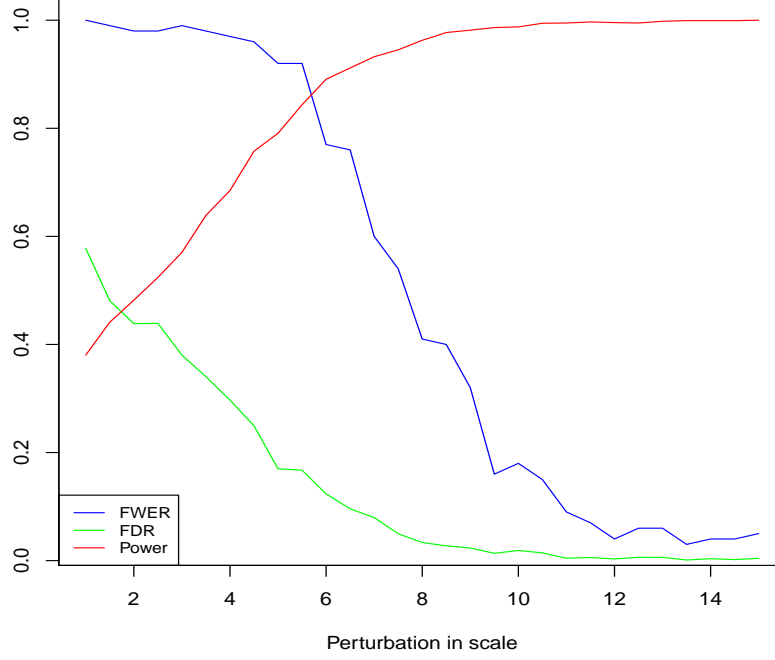


FIGURE 2. FWER, FDR and power of the GFS algorithm using the MMCM test in the scale setting

$$\begin{aligned}
 &\text{mean of } i\text{th feature} && \text{Covariance of } i\text{th feature between classes } i \text{ and } k \\
 \mu^{(i)} = \begin{cases} 0 & \text{if } i \notin L \\ i\theta & \text{if } i \in L \end{cases} && \Sigma_{jk}^{(i)} = \begin{cases} \rho, & \text{if } j \notin L \text{ and } k \notin L \text{ and } j \neq k \\ 1, & \text{if } j \notin L \text{ and } k \notin L \text{ and } j = k \\ \rho(1 + (i-1)\phi) & \text{if } j \in L \text{ and } k \in L \text{ and } j \neq k \\ 1 + (i-1)\phi, & \text{if } j \in L \text{ and } k \in L \text{ and } j = k \\ \rho, & \text{otherwise} \end{cases}
 \end{aligned}$$

where L is a randomly chosen subset of $\{1, \dots, d\}$. We take $\theta \in \{0, 0.1, 0.2, \dots, 0.7\}$ and $\phi \in \{0, 1, 3, 5, \dots, 15\}$ for $\rho = 0.1$. $\theta = 0$ corresponds to no shift in location and $\phi = 0$ corresponds to no shift in scale. We compare our method with a test developed by Kruskal and Wallis [7, 8], a distribution-free test, which is a K sample analogue of the Mann-Whitney test. To select the set of important variables using the Kruskal Wallis test, we performed a univariate test and did a multiplicity correction. We plot the empirical FWER, FDR and power calculated over 30 replicates.

We observe that the Kruskal Wallis test does not detect any change in scale. However, in absence of any scale change, it performs better in detecting a location shift, even in low signal domain. This is expected as the Kruskal Wallis test is powerful in location shift set ups only.

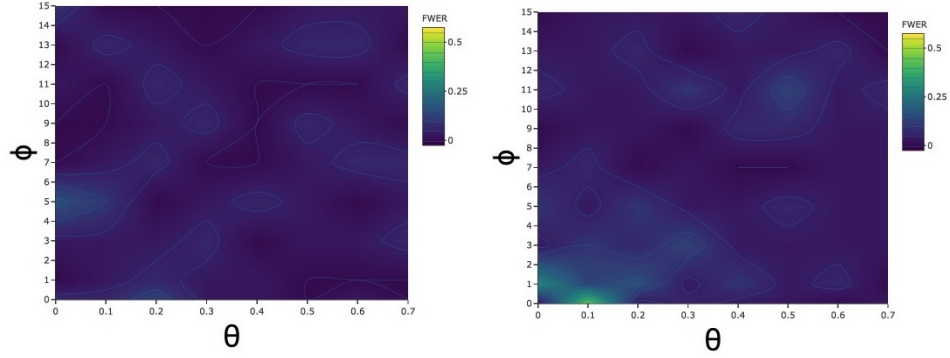


FIGURE 3. Contour plot of FWER of Kruskal Wallis (left panel) and the GFS algorithm (right panel)

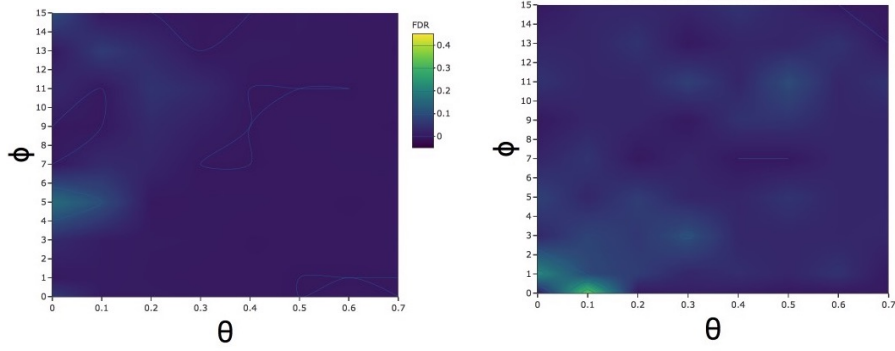
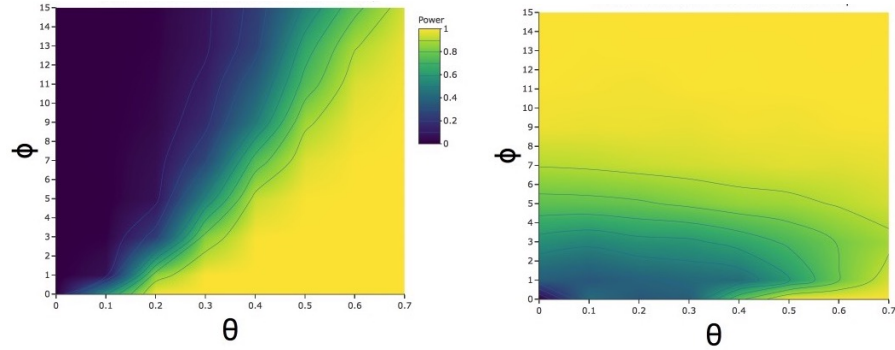


FIGURE 4. Contour plot of FDR of Kruskal Wallis (left panel) and the GFS algorithm (right panel)



GFS has a high false discovery rate for extreme values of θ and ϕ (location and scale shift)

FIGURE 5. Contour plot of power of Kruskal Wallis (left panel) and the GFS algorithm (right panel)

Next we consider a simulation set up where the samples do not come from the same parametric family.

4.4. Comparison with the Kruskal Wallis test in different parametric families: In this set up we take $K = 3$, i.e., we assume that the data is coming from 3

different classes. For each of the distributions F_1, F_2 and F_3 , the last $d - \lceil \frac{d}{4} \rceil$ marginals are taken to be independent standard Gaussian. As for the first $\lceil \frac{d}{4} \rceil$ marginals they are assumed to be sampled independently from a multivariate standard Gaussian distribution for F_1 , multivariate standard Cauchy distribution for F_2 and multivariate standard t distribution for F_3 . For this simulation, we set each of the class sizes at 400. We varied d within $\{50, 75, 100, \dots, 250\}$. The degrees of freedom of the multivariate t distribution was taken to be 7. In table 1, we compare the performance of Kruskal Wallis and our proposed GFS algorithm.

$p \downarrow$	FWER of GFS	Power of GFS	Power of Kruskal Wallis
50	0.0667	0.6128	0.0000
75	0.0333	0.5667	0.0000
100	0.1333	0.5814	0.0000
125	0.0000	0.5667	0.0000
150	0.0667	0.5447	0.0009
175	0.0333	0.5326	0.0008
200	0.0333	0.5160	0.0000
225	0.0000	0.5211	0.0006
250	0.0333	0.5138	0.0005

GFS has much better power when there are more parameters

TABLE 1. Different parametric family: power

We do not tabulate FWER and FDR of Kruskal Wallis test as they are nearly 0.

5. REAL DATA ANALYSIS

In this section, we show the performance of our GFS algorithm on several real datasets.

5.1. Portugal Forest Fires Data. The Portugal forest fires data <http://archive.ics.uci.edu/ml/datasets/Forest+Fires> (also see [23]) describes several meteorological features of a number of locations in Montesinho natural park, from the Trás-os-Montes northeast region of Portugal, and provides a measure of the areas burnt by forest fires in each of these locations. This dataset contains 517 instances, collected over a period of four years (2000-2004). Whenever a forest fire broke out, the following spatio-temporal and meteorological information were collected: *spatial locations* (x and y coordinates), *date of occurrence*, *Fine Fuel Moisture Code (FFMC)*, *Duff Moisture Code (DMC)*, *Drought Code (DC)*, *Initial Spread Index (ISI)*, *temperature*, *relative humidity (RH)*, *wind speed*, *rain*, and *area burnt*.

In our analysis, we included all the above attributes except *date of occurrence* and *area burnt* as relevant features, giving us a total of 10 univariate features. The variable *area burnt* was used as a classifier, and since its histogram has a huge peak at 0, we discretized its range into two classes: 0 and positive. We then used the GFS algorithm

to identify which of the 10 features would be most informative about whether an area is burnt.

The GFS algorithm picked six of the 10 features, namely all the component variables of the Fire Weather Index (FWI) system: FPMC, DMC, DC, ISI, and the two weather attributes: temperature and wind, as significant variables. On the contrary, when the Kruskal Wallis test was applied to each of the 10 features and a multiple hypothesis testing correction was applied, none of the 10 variable met the threshold of 0.05 for statistical significance. This, in turn, indicates a greater detection power of the multi-sample graph-based tests in the generality. In fact, the smallest p-value reported by the univariate Kruskal-Wallis test is 0.017, which is larger than the Bonferroni multiple-comparison level of 0.005.

5.2. Single Cell Transcriptomics Data. Feature selection is especially important in modern biomedical research, where high-throughput and multi-dimensional datasets are becoming increasingly prevalent with recent advances in single cell technologies [24]. For instance, to characterize novel cellular states, single cell RNA sequencing (scRNA-seq) is used in exploratory analyses; scRNA-seq data analysis procedures such as cell type clustering or dimension reduction are often driven by select gene expression profiles. Appropriate feature selection in this domain has major implications on how differences or similarities are estimated between pairs of cells, subsequently affecting any downstream methods [25, 26]. Selection of differentially expressed genes or highly variable features, therefore, holds utmost importance for both computational efficiency and for drawing meaningful scientific inferences from the data [24, 25].

Existing methods of feature selection in scRNA-seq data analysis select features by deviance, or the most highly variable genes. In contrast, we sought to use the GFS algorithm to select differentially distributed features that can help inform the underlying biology. We employed our algorithm in a multi-sample setting of relevant human memory CD4 T cell biology. We used an existing dataset of purified human memory CD4+ T cells, which were either left unstimulated (0 hr), or CD3/CD28 stimulated for 12 or 24 hours (12hr and 24hr, respectively). scRNA-seq was then performed on the cell populations at each of the three different time points [17]. In a dataset where the goal is to compare multiple time points concurrently to identify the features of interest, existing methods take a two-sample approach (comparing two time points at a time), which tends to decrease the power and sensitivity of the analysis. In GFS, we circumvent this problem by harnessing a multisample and multivariate graph based test as the basis.

In order to have the recursion depth of our algorithm within control, we divided the set of features (genes) in the dataset into 8 groups of equal size based on a pivot-based clustering approach. To elaborate, for every variable i and every $\rho \in (0, 1)$, we define $N_\rho(i)$ to be the set of all variables other than i , which have Spearman correlation at least ρ with i , and select that variable i , for which the size of $N_\rho(i)$ is maximum, which we call a pivot. We then include the variables with highest correlation with the pivot i in the first group. After constructing the first group, we leave it out subsequently, and apply the same mechanism on the remaining variables (by choosing a pivot from the left-out variables, and including in the second group the variables from among

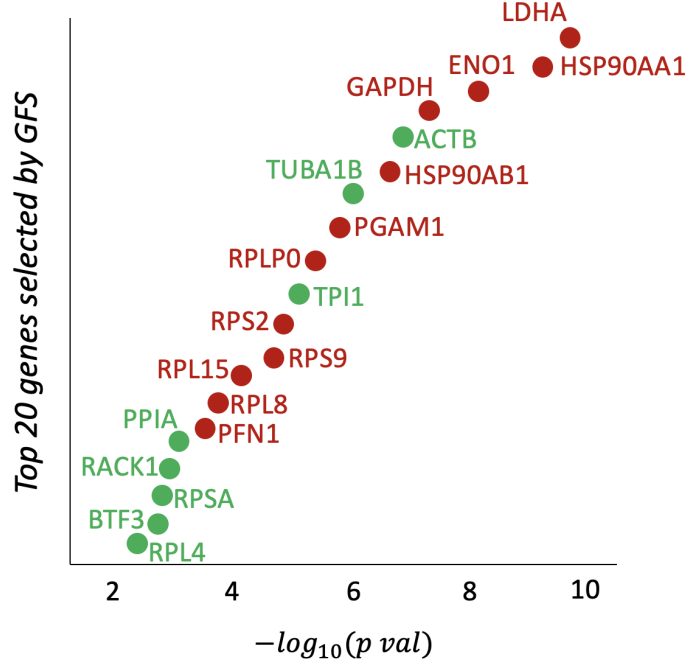


FIGURE 6. Top 20 differentially distributed genes between resting and activated human memory CD4 T cells. GFS detects known biologically important genes (in red) while also detecting new features of interest (genes labeled in green)

the remaining ones, whose correlation with this second step pivot is maximum). We continue this process till the eighth and final group has been constructed. We take $\rho = 0.5$ in our analysis, and if $N_{0.5}(i)$ happens to be empty for some pivot i , we reduce ρ in decrements of 0.05, till $N_{\rho}(i)$ becomes non-empty. Next, within each group, we carry out our MMCM test over 1000 bootstrap iterations on randomly selected sub-samples of equal size from each class, in each of these iterations. Finally, we report the features that get selected across each of the 1000 bootstrap iterations.

Utilizing the GFS approach to identify differentially distributed genes in the single cell transcriptomics setting, we discovered a variety of genes with both known and previously unrecognized roles in T cell biology (Fig. 6). For example, activated memory CD4 T cells rely on export of metabolites from the mitochondria to support epigenetic remodeling required for effector functions. Lactate dehydrogenase A (LDHA) in particular is known to be critical for glycolysis in CD4 T cells [27, 28]. Interestingly, glycolytic enzymes such as phosphoglycerate mutase-1 (PGAM1) and LDHA, as well as heat shock protein 90 (HSP90) molecules were found to be among the top 10 differentially distributed genes across the three subgroups based on GFS. Not only did our algorithm recapitulate aspects of known biology, but also highlighted previously unrecognized molecules such as receptor for activated c kinase 1 (RACK1) and basic

transcription factor 3 (BTF3), which might play an important role in memory CD4 T cell activation.

5.3. Mice Protein Data.

5.3.1. *Dataset Introduction.* The *Mice Protein dataset* contains the expression level data of 77 protein markers in mice, which are generated from an experiment aiming to detect the important proteins that contribute to learning. As shown in Figure 7, the dataset is classified into 8 classes according to three aspects, namely the genotype of mice, stimulation behavior and drug treatment, which may lead to different learning outcomes. The dataset contains a total of 1080 measurements of protein response, each considered as an independent sample.

Classes	Genotype	Behavior	Drug treatment	Learning Outcome	# of Mice
c-CS-s	control mice	stimulated to learn	saline	Normal	9 mice
c-CS-m	control mice	stimulated to learn	memantine	Normal	10 mice
c-SC-s	control mice	not stimulated to learn	saline	No learning	9 mice
c-SC-m	control mice	not stimulated to learn	memantine	No learning	10 mice
t-CS-s	trisomy mice	stimulated to learn	saline	Failed	7 mice
t-CS-m	trisomy mice	stimulated to learn	memantine	Rescued	9 mice
t-SC-s	trisomy mice	not stimulated to learn	saline	No learning	9 mice
t-SC-m	trisomy mice	not stimulated to learn	memantine	No learning	9 mice

FIGURE 7. Classes of mice

5.3.2. *Data Pre-processing.* We first examined the basic data structure and filtered out 528 missing values. From Figure 8, we can see that the 8 classes of samples are unbalanced.

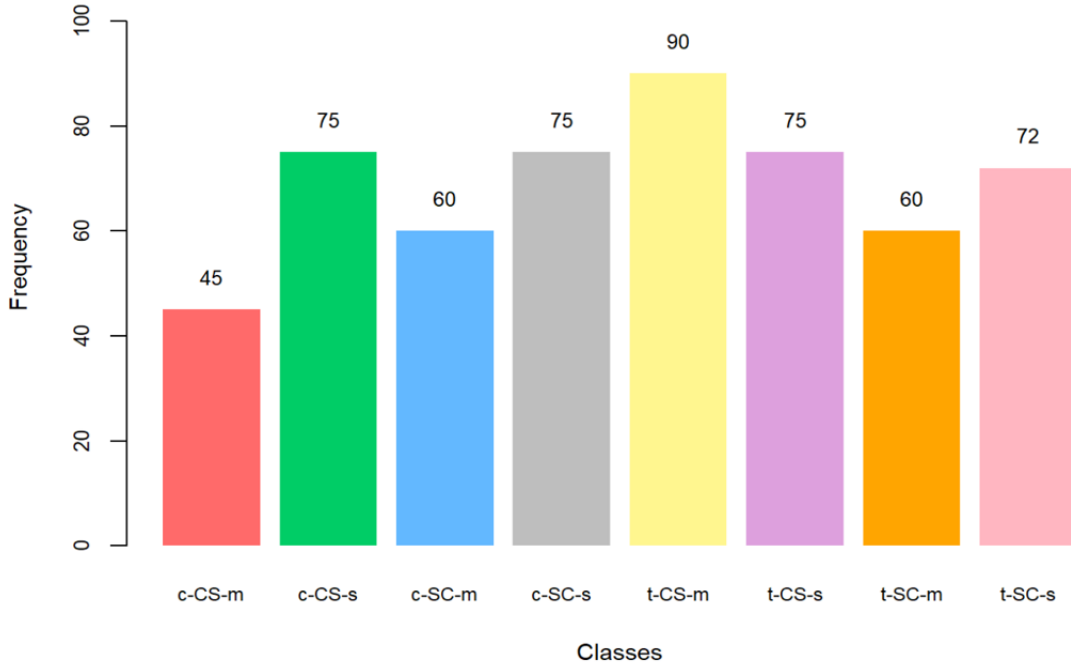


FIGURE 8. Frequency distribution of mice classes

Figure 9 shows that some features might not be normally distributed. However, since the MCM and MMCM tests are non-parametric and distribution-free, no distributional assumptions will be needed.

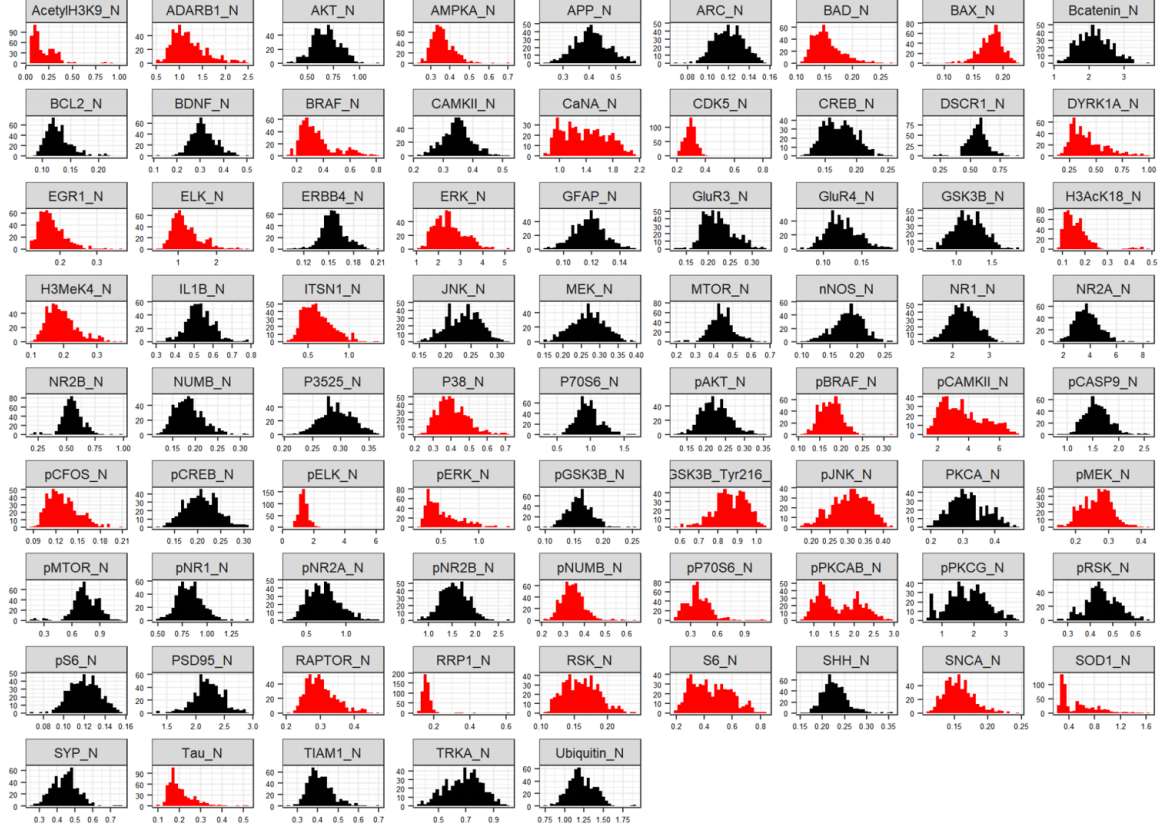


FIGURE 9. Feature distributions
77 protein markers

As Figure 10 suggests, the majority of protein expression levels are highly correlated. To determine whether a significant difference exists between the 8 classes, we sought to find out the pivotal proteins that might be contributing to the overall difference, which in turn may help to detect the latent effective drug targets.

5.3.3. Feature Selection Based on the MMCM Test. To detect the difference between 8 mice classes, we first applied the MMCM test, and the test statistic turns out to be 1679.85, much larger than $\chi^2_{0.95}(28) = 41.34$. So the null hypothesis of no difference can be rejected at level 0.05, thereby enabling us to conclude that there exists a statistical difference between 8 classes.

Based on the MMCM test result, we further employ the GFS algorithm to identify the most important proteins that contributed to the overall difference in learning outcomes of mice and also employ two traditional parametric methods for comparison. The GFS approach selects 47 significant proteins and Figure 11 lists the top 30 based on the MMCM test p-values.

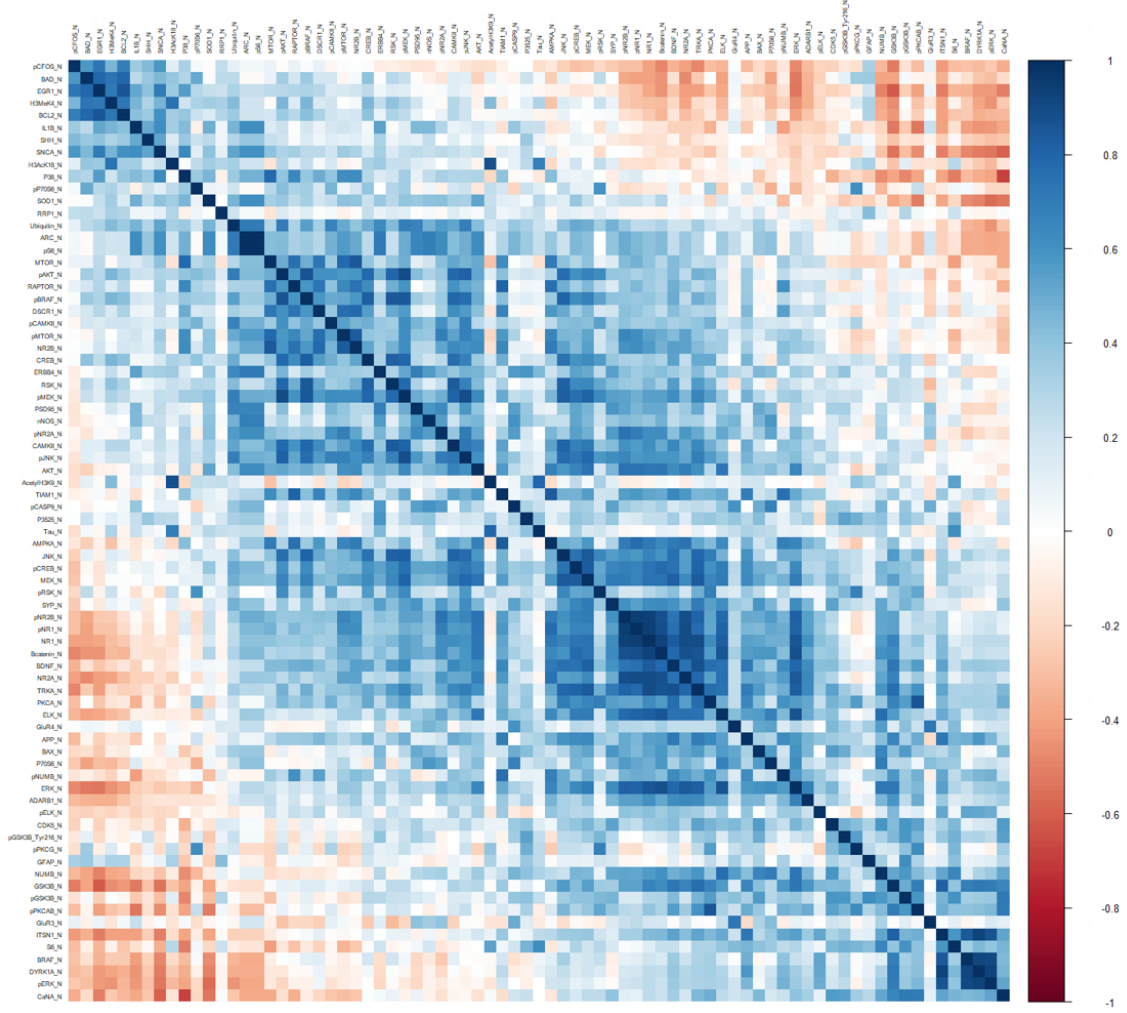


FIGURE 10. Correlation between features

5.3.4. *Multinomial Logistic Regression with LASSO (MLR-LASSO)*. We first standardized all the features based on their data distribution. Given the high correlation between most features, we incorporated the L^1 regularization method, namely LASSO (Least Absolute Shrinkage and Selection Operator), to establish a multinomial logistic regression model. LASSO is capable of both regularization and feature selection. This method gives 8 regression models on 8 classes and we subsequently select 31 important proteins in total as shown in Figure12. In addition, we test the model on 30% samples and gain an accuracy of approximately 87.35%.

5.3.5. *Random Forest (RF)*. This approach gets the Feature Importance Score according to mean decrease in Gini coefficient and we take the top 40 important features in consideration as shown in Figure 13. We also test this model on 30% samples and achieve an accuracy of nearly 97.59%.

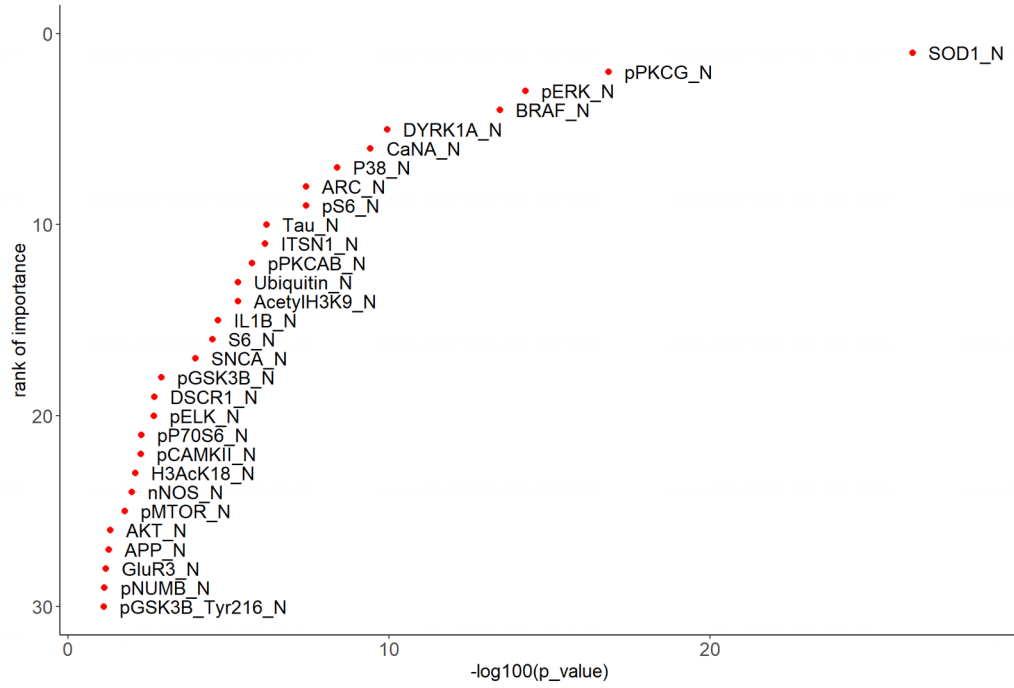


FIGURE 11. Top 30 proteins selected by GFS

c-CS-m		c-CS-s		c-SC-m		c-SC-s	
Intercept	0.0149	Intercept	0.2401	Intercept	-0.1409	Intercept	-0.2326
BAX_N	-0.2472	APP_N	-0.3345	CaNA_N	-0.6747	AKT_N	0.6795
BCL2_N	-0.4481	BAX_N	0.0162	EGR1_N	0.0068	pNUMB_N	-0.4746
P3525_N	0.3717	CaNA_N	0.5894	GluR3_N	0.5677	S6_N	-0.2449
pERK_N	0.1197	ERK_N	0.0053	IL1B_N	0.2117	SOD1_N	0.6102
		pAKT_N	-0.2576	pCAMKII_N	0.1129		
		pCAMKII_N	-0.0434				
		pGSK3B_N	0.0780				
		pNUMB_N	0.5771				
t-CS-m		t-CS-s		t-SC-m		t-SC-s	
Intercept	0.0582	Intercept	0.0608	Intercept	-0.1443	Intercept	0.1436
ARC_N	-0.1887	APP_N	0.6548	ARC_N	0.4875	P3525_N	0.0896
BRAF_N	1.4527	NR2B_N	-0.2991	GFAP_N	-0.0193	pGSK3B_Tyr216_N	0.1714
CaNA_N	0.2690	P38_N	-0.9709	GluR4_N	-0.0113	pP70S6_N	0.0432
pP70S6_N	0.0536	pCAMKII_N	-0.1248	H3AcK18_N	0.5103	pPKCG_N	0.8298
pS6_N	-0.0725	S6_N	0.0734	pS6_N	0.2090	RAPTOR_N	0.0152
				Tau_N	0.1089	SOD1_N	0.5433
				Ubiquitin_N	0.1605	Tau_N	0.4266

FIGURE 12. Proteins selected by Multinomial Regression with LASSO

5.3.6. *Result Analysis.* The common important features (proteins) selected by the above three methods are listed in Figure 14. As shown in Figure 15, the highly correlated feature pairs in the original dataset would be reduced by employing the feature selection methods. The common selected proteins are expected to be the most important features. Furthermore, according to the rank of importance given by both the GFS and

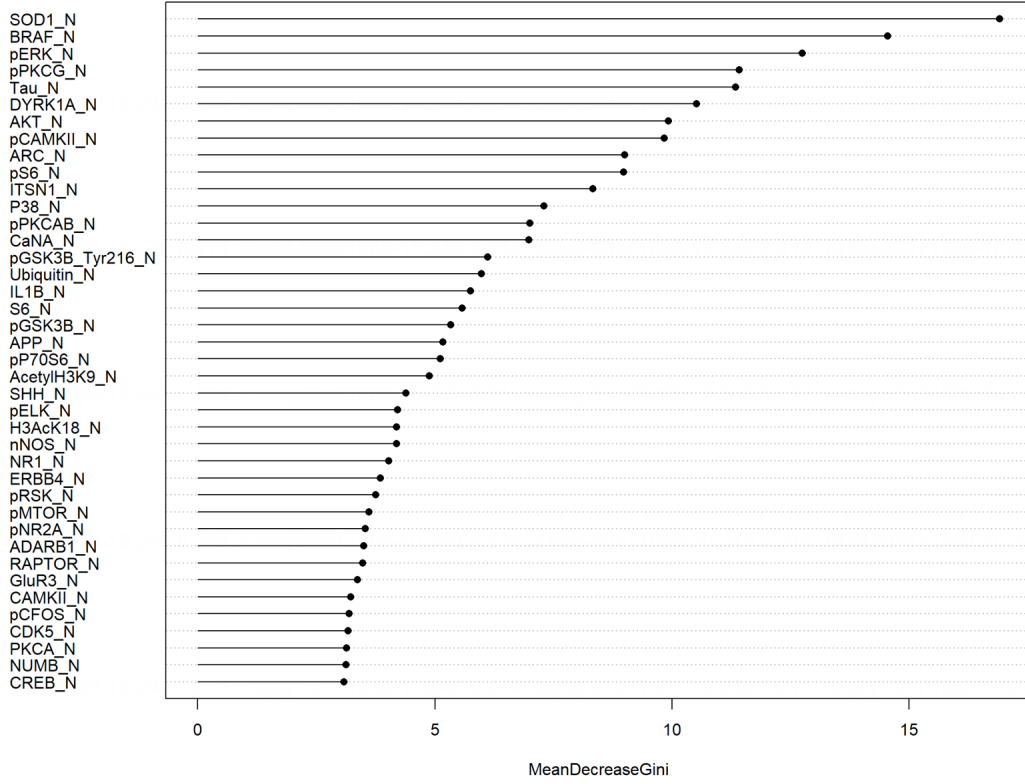


FIGURE 13. Feature importance of top 40 proteins

the Random Forest method (see Figure 14), proteins ranked highly by both methods can be surmised as more effective drug targets.

5.4. Brain Cancer Data.

5.4.1. Dataset Introduction. The *Brain Cancer dataset* is publicly available from the Gene Expression Omnibus (GEO) data base [29], and comprises of a transcriptomics study to explore the underlying relationship between various genes and the difference among types of brain tumors. The gene expression profiles of 130 surgical tumor and normal brain samples were obtained via Affymetrix HG-U133plus2 chips. To isolate the gene expression of pivotal immune cell markers, the gene expression profiles of various types of brain tumors and normal brains were filtered. Nearly 56,000 genes were profiled in total and all samples were labeled in 5 classes, namely ependymoma, glioblastoma, medulloblastoma, normal, and pilocytic astrocytoma. An example of some of the genes included with corresponding representative gene IDs and titles are shown in Figure 16.

5.4.2. Data Pre-Processing. Considering there are over 56,000 genes in the brain cancer dataset, applying our GFS method would be inherently challenging due to computational resources. Hence we pre-selected highly variable genes based on their expression level by using Median Absolute Difference (MAD):

$$\text{MAD} = \text{median}_i(\text{median}_j |S_{i,j} - \bar{S}_i|)$$

	Common_Feature	Rank_of_GFS	Rank_of_Random_Forest
1	SOD1_N	1	1
2	pPKCG_N	2	2
3	pERK_N	3	4
4	BRAF_N	4	3
5	CaNA_N	6	6
6	P38_N	7	10
7	ARC_N	8	15
8	pS6_N	9	18
9	Tau_N	10	8
10	Ubiquitin_N	13	24
11	IL1B_N	15	23
12	S6_N	16	19
13	pGSK3B_N	18	12
14	pP70S6_N	21	22
15	pCAMKII_N	22	7
16	H3AcK18_N	23	28
17	AKT_N	26	13
18	APP_N	27	16
19	Glur3_N	28	14
20	pNUMB_N	29	21
21	pGSK3B_Tyr216_N	30	20
22	NR2B_N	39	55
23	pAKT_N	40	48
24	BCL2_N	41	70
25	EGR1_N	42	63

FIGURE 14. Common features selected by GFS and RF

Feature Selection Method	None	GFS	MLR-LASSO	RF	Common Selected
Correlation > 0.4	29.80%	28.40%	21.72%	22.18%	24.00%
Correlation > 0.8	2.05%	1.85%	0.65%	1.03%	1.00%

FIGURE 15. Proportion of highly related feature pairs

ID	Species Scientific Name	Representative Public ID	Gene Title
1007_s_at	Homo sapiens	U48705	discoidin domain receptor tyrosine kinase 1 /// microRNA 4640
1053_at	Homo sapiens	M87338	replication factor C (activator 1) 2, 40kDa
117_at	Homo sapiens	X51757	heat shock 70kDa protein 6 (HSP70B')
121_at	Homo sapiens	X69699	paired box 8
1255_g_at	Homo sapiens	L36861	guanylate cyclase activator 1A (retina)
1294_at	Homo sapiens	L13852	microRNA 5193 /// ubiquitin-like modifier activating enzyme 7
1316_at	Homo sapiens	X55005	thyroid hormone receptor, alpha
1320_at	Homo sapiens	X79510	protein tyrosine phosphatase, non-receptor type 21

FIGURE 16. Description of gene probes in the brain cancer dataset

where S_{ij} , $i = 1, \dots, 56000$, $j = 1, \dots, 130$ are values in the (i, j) -th entries in the gene expression matrix and \mathbf{S}_i is the median of $(S_{i,j})_{j \geq 1}$. We re-ordered all genes and selected the first 5000 with the largest MAD for downstream analyses.

5.4.3. Structure of dataset. After pre-selecting genes, we performed exploratory data analysis. The left window of Figure 17 shows the expression value distribution plot for 5,000 genes. These distributions have clear dissimilarities in terms of means and variances, as is revealed by the plots. The right window of Figure 17 shows the mean and variance trend of all the 5,000 variables. These data points show a clear pattern, thereby suggesting a quantifiable biological structure, which we expect to be picked up in our feature selection algorithm.

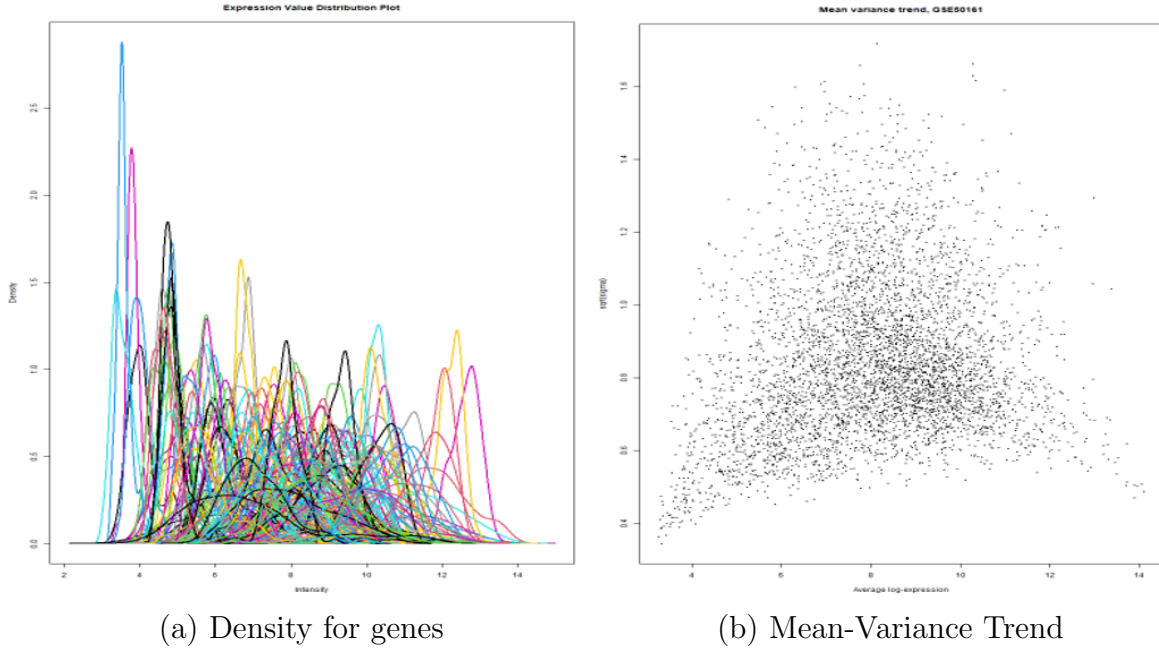


FIGURE 17. EDA on Brain Cancer dataset

5.4.4. Pre-Clustering. Genes can be co-expressed as part of a shared chemical or biological function. To capture this, we decided to apply Weighted Gene Co-expression Network Analysis (WGCNA)[30]. It is a widely used systems biology method for constructing a co-expression network based on the expression matrix of various genes, and allowed us to cluster genes into different key modules. By applying this method, we divided our 5,000 genes into 23 modules where each module corresponds to a particular biological pathway.

5.4.5. Results Summary. We applied the MMCM test to the $130 \times 5,000$ data matrix. We observed that the MMCM test statistic was much greater than $t_{8385}(0.05)$, indicating that the differences among various types of brain tumors were significant. Next, we applied our GFS method to each of the 23 modules to select the most significant variables within them. We set the significance level to 0.05 and selected a total of 935

variables. The results of this analysis are illustrated in Figure 18. From the bar chart, we can see that in Module 8, we did not select any features from the 22 genes included in that module. This could be due to our choice of significance level, or it could be because Module 8 has unique characteristics that make it less informative for identifying significant variables.

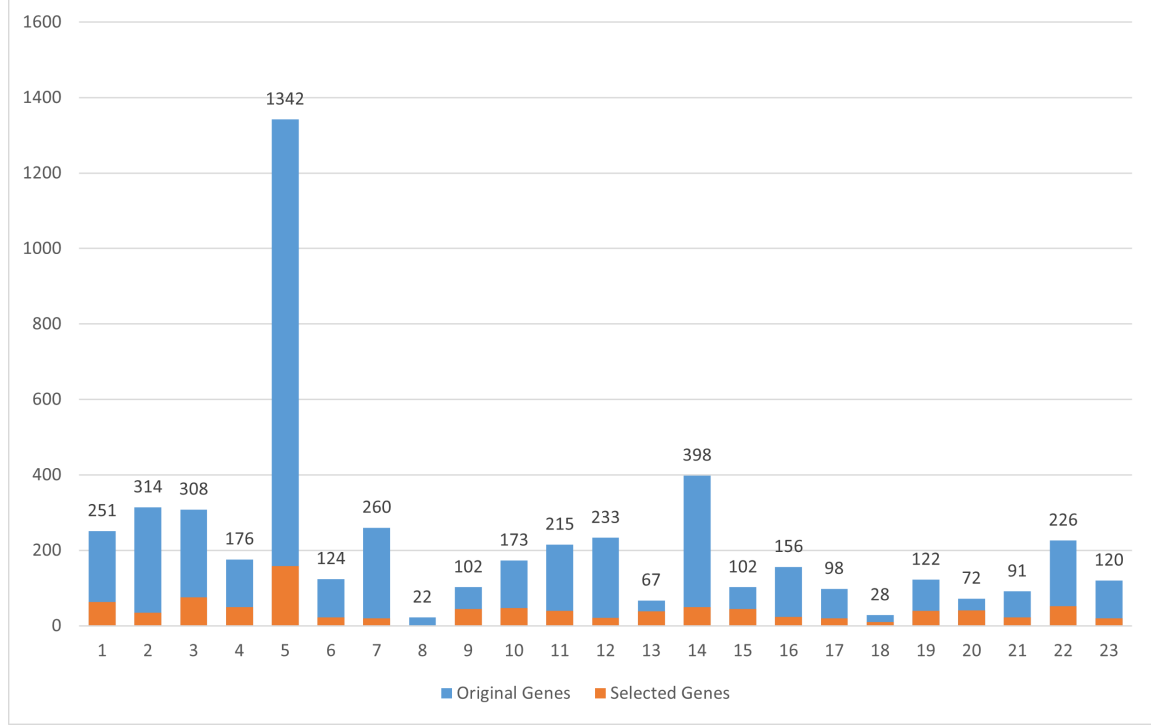


FIGURE 18. Bar chart for selected variables

To gain further insight into the relationship between types of brain tumors and our selected genes, we sorted the variables by their corresponding adjusted p -values, from small to large. This approach allows us to focus on genes that have a high degree of confidence in differentiating between tumor types and have a greater contribution during cellular processes. Figure 19 shows the first 5 genes that were sorted. Interestingly, all of these genes belong to Modules 9 and 10, which are likely related to brain tumors, as confirmed by Gene Ontology (GO) enrichment analysis [31], a method for identifying over-represented biological functions or processes associated with a set of genes or proteins of interest. This analysis suggests that most genes in these modules have functions related to birth processes (germline mutations), which are important in the development of brain tumors.

To evaluate the performance of our GFS method, we compared it with other common feature selection methods, namely Multinomial regression based on LASSO and Random Forest. We use SVM with RBF kernel as our classification model and apply it to the selected features. We divide our samples into training and test datasets with a proportion of 0.7 for the training dataset. During the training procedure, we perform a grid search to find the best hyperparameters to avoid overfitting. The results of

Probes	RefSeq	Module ID	Module name	GO enrichment analysis
208017_s_at	NM_005369	9	greenyellow	Birth Process
202986_at	0003677	9	greenyellow	Birth Process
214768_x_at	0003823	10	grey60	Birth Process, Cellular Component
206477_s_at	NM_002516	10	grey60	Birth Process, Cellular Component
222078_at	0000166	9	greenyellow	Birth Process

FIGURE 19. Table for top 5 genes

Probes	Gene Name	Description
208017_s_at	PAFAH1B1	It is involved in mitosis and intracellular transport. Mutations in this gene have been linked to several neurodevelopmental disorders, such as lissencephaly
222078_at	Tumor Necrosis Factor (TNF)	It is a cytokine produced by immune cells and is involved in a variety of biological functions such as inducing apoptosis in tumor cells

FIGURE 20. Formal description of original genes

our comparison are shown in Figure 21. The GFS method outperforms other feature selection methods in terms of validation accuracy, thereby suggesting that the combination of the MMCM test and the GFS algorithm might serve as a more efficient and applicable approach.

Overall, our study provides a promising approach for identifying significant genes in brain tumor classification and demonstrates the effectiveness of our GFS method in feature selection for classification models.

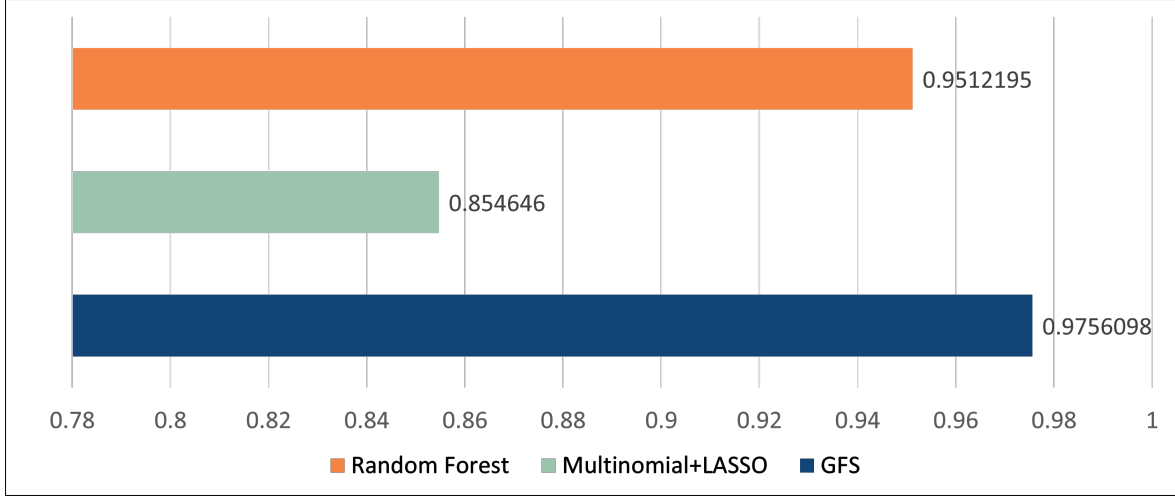


FIGURE 21. Comparison between common feature selection methods

6. DISCUSSION

In this paper, we describe a graph-based hierarchical clustering approach for multi-dimensional feature selection under a complete nonparametric multisample setup. This method, which we call the GFS algorithm, is consistent, i.e., it reports all the true features contributing to the distributional difference with high probability. Concurrently, GFS guarantees a control on the probability of selecting at least one non-contributing feature. Our simulations show that this graph-based approach provides a substantial improvement over classical parametric tests for location shift, such as the Kruskal Wallis test, in the generality. Further still, through analysis of the Portuguese forest fires data, a single cell transcriptomics data, a mice protein data and a brain cancer data, we highlight the power of GFS at unearthing and capturing variables that can provide deeper insights into the process being examined. With growing popularity of scRNA-seq data in biomedical research, we envision that our method can find a unique place in instances wherein multiple cell types of patient cohorts are being compared, and existing differential gene expression methods find limited utility.

At the heart of our feature-selection method is the nonparametric multisample graph-based testing approach. We would like to emphasize that the hierarchical clustering procedure is just a tool, and can be replaced by other suitable alternatives. For example, a potentially promising alternative may be to implement a “bootstrap” type of algorithm, where the basic idea is to select a certain number of random subsets of a fixed cardinality from the feature set, and carry out the multisample graph-based test on the sub-datasets obtained by truncating the original dataset at those random feature subsets. All the significant sub-datasets are then pooled together keeping track of the multiplicity of each feature appearing in the pooled multiset. The variables in this pooled multiset can then be reported as significant features, in decreasing order of their multiplicities. Establishing theoretical guarantees for the bootstrap approach may be an interesting direction for future research. Nonetheless, in this work we establish that multivariate graph-based methods can be powerful tools for developing feature

selection algorithms that detect meaningful features which might not be captured by existing univariate approaches.

7. ACKNOWLEDGMENT

S.G. was supported by the National Science Foundation BIGDATA grant IIS-1837931. S.M. was supported by the National University of Singapore start-up grant WBS A0008523-00-00 and the Faculty of Science Tier 1 grant WBS A-8001449-00-00. We are immensely grateful to Nancy Zhang for suggesting us this problem and giving some nice ideas to attack it, including the alternative bootstrap-type approach. We would also like to thank Bhaswar Bhattacharya for several helpful discussions throughout the preparation of this manuscript.

8. APPENDIX

In this section, we prove some technical lemmas necessary for the proof of Theorem 1, and show exact numerical results for some of the simulations we did earlier.

8.1. Technical Results. In this section, we prove some technical results needed to prove Theorem 1.

Lemma 1. *A signal set is unique.*

Proof. Suppose that L_1 and L_2 are two signal sets. It is enough to show that $L_1 \subseteq L_2$, since the other inclusion will then follow by symmetry. Towards showing this, take $i \in L_1$. By (2), $H_{0,\{i\}}$ is not true, i.e. there exist $1 \leq u < v \leq K$ such that $F_{u[\{i\}]} \neq F_{v[\{i\}]}$. This means that for all $L \supseteq \{i\}$, $F_{u[L]} \neq F_{v[L]}$, and hence, $H_{0,L}$ is not true, and therefore, by (1), $L \neq L_2^c$. We conclude that $i \notin L_2^c$, i.e. $i \in L_2$. This completes the proof. \square

Lemma 2. *Let $\mathcal{T}_0 := \{C \in \mathcal{T} : H_{0,C} \text{ is true}\}$, and let $\mathcal{T}_{\text{rej}} := \{C \in \mathcal{T} : \max_{U \in \mathcal{T} : U \supseteq C} p_{\text{adj}}^U \leq \alpha\}$. Then,*

$$\mathbb{P}(\mathcal{T}_0 \cap \mathcal{T}_{\text{rej}} \neq \emptyset) \leq \alpha .$$

Proof. The proof of Lemma 2 is exactly similar to the proof of Theorem 1 in [12], but since the framework there is a regression setup, we replicate their argument and show that everything remains unchanged even in our nonparametric setup. To start with, let us define:

$$\mathcal{T}_0^{\max} := \{C \in \mathcal{T}_0 : \nexists V \in \mathcal{T}_0 \text{ with } V \supseteq C\} .$$

Now, it is evident that:

$$\{\mathcal{T}_0 \cap \mathcal{T}_{\text{rej}} \neq \emptyset\} = \{\mathcal{T}_0^{\max} \cap \mathcal{T}_{\text{rej}} \neq \emptyset\} \subseteq \{\mathcal{T}_0^{\max} \cap \{C \in \mathcal{T} : p_{\text{adj}}^C \leq \alpha\} \neq \emptyset\} .$$

Hence, we have:

$$\mathbb{P}(\mathcal{T}_0 \cap \mathcal{T}_{\text{rej}} \neq \emptyset) \leq \sum_{C \in \mathcal{T}_0^{\max}} \mathbb{P}(p_{\text{adj}}^C \leq \alpha) = \sum_{C \in \mathcal{T}_0^{\max}} \frac{\alpha |C|}{d} .$$

Since any two distinct elements of \mathcal{T}_0^{\max} are disjoint, it follows that:

$$\sum_{C \in \mathcal{T}_0^{\max}} |C| \leq d .$$

Hence, we have:

$$\mathbb{P} \left(\mathcal{T}_0 \cap \mathcal{T}_{\text{rej}} \neq \emptyset \right) \leq \alpha ,$$

completing the proof of Lemma 2. □

8.2. Numerics for location and scale families : In this section, we tabulate the exact numerical results for the simulations in Sections 4.1 and 4.2.

$\theta \downarrow$	FWER	FDR	Power
.15	0.45	0.08	0.33
.20	0.04	0.01	0.31
.25	0.07	0.02	0.35
.30	0.04	0.005	0.41
.35	0.03	0.003	0.51
.40	0.04	0.003	0.80
.45	0.05	0.003	0.97
.50	0.03	0.001	1.00
.55	0.03	0.004	1.00
.60	0.03	0.001	1.00
.65	0.02	0.004	1.00
.70	0.02	0.004	1.00
.75	0.03	0.006	1.00

TABLE 2. Location Setting: FWER, FDR and Power

$\theta \downarrow$	FWER	FDR	Power
1.0	1.00	0.58	0.38
1.5	0.99	0.48	0.44
2.0	0.98	0.44	0.48
2.5	0.98	0.44	0.52
3.0	0.99	0.38	0.57
3.5	0.98	0.34	0.64
4.0	0.97	0.30	0.68
4.5	0.96	0.25	0.76
5.0	0.92	0.17	0.79
5.5	0.92	0.17	0.84
6.0	0.77	0.12	0.89
6.5	0.76	0.10	0.91
7.0	0.6	0.08	0.93
7.5	0.54	0.05	0.95
8.0	0.41	0.03	0.96
8.5	0.40	0.03	0.977
9.0	0.32	0.02	0.982
9.5	0.16	0.01	0.986
10.0	0.18	0.02	0.988
10.5	0.15	0.01	0.994
11.0	0.09	0.004	0.995
11.5	0.07	0.006	0.997
12.0	0.04	0.003	0.996
12.5	0.06	0.006	0.995
13.0	0.06	0.006	0.998
13.5	0.03	0.001	0.999
14.0	0.04	0.004	0.999
14.5	0.04	0.002	0.999
15.0	0.05	0.004	1

TABLE 3. Scale Setting: FWER, FDR and Power

REFERENCES

- [1] P. J. Bickel, A distribution free version of the Smirnov two sample test in the p -variate case, *Annals of Mathematical Statistics*, Vol. 40, 1–23, 1969.
- [2] M. Biswas, M. Mukhopadhyay, and A. K. Ghosh, A distribution-free two-sample run test applicable to high-dimensional data, *Biometrika*, 101(4):913–926, 10 2014.
- [3] J. H. Friedman and L. C. Rafsky, Multivariate generalizations of the Wald-Wolfowitz and Smirnov two-sample tests, *Ann. Statist.*, 7(4):697–717, 07 1979.
- [4] M.H. Chehreghani, Hierarchical Correlation Clustering and Tree Preserving Embedding, arXiv:2002.07756, 2020.
- [5] J. D. Gibbons and S. Chakraborty, *Nonparametric Statistical Inference*, Fourth Edition. Marcel Dekker Inc., 2003.

- [6] T. Hastie, R. Tibshirani, J. Friedman, The Elements of Statistical Learning; Data Mining, Inference and Prediction. New York, Springer, 2001.
- [7] W. H. Kruskal. A nonparametric test for the several sample problem, *Ann. Math. Statist.*, 23(4):525–540, 12 1952.
- [8] W. H. Kruskal and W. A. Wallis, Use of ranks in one-criterion variance analysis, *Journal of the American Statistical Association*, 47(260):583–621, 1952.
- [9] H. B. Mann and D. R. Whitney, On a test of whether one of two random variables is stochastically larger than the other, *Annals of Mathematical Statistics*, Vol. 18(1), 50–60, 1947.
- [10] S. C. Johnson, Hierarchical clustering schemes *Psychometrika*, Vol. 32(3), 241–254, 1967.
- [11] D. Zhu, D. P. Guralnik, X. Wang, X. Li and B. Moran Statistical properties of the single linkage hierarchical clustering estimator. *Journal of Statistical Planning and Inference*, Vol. 185, 15–28, 2017.
- [12] N. Meinshausen. Hierarchical testing of variable importance, *Biometrika*, 95, 2, 265–278, 2008.
- [13] Daniel Müllner. Modern hierarchical, agglomerative clustering algorithms, arXiv:1109.2378, 2011
- [14] S. Mukherjee, D. Agarwal, N. Zhang and B.B. Bhattacharya, Distribution-free Multisample Test Based on Optimal Matching with Applications to Single Cell Genomics, *Journal of the American Statistical Association*, <https://doi.org/10.1080/01621459.2020.1791131>
- [15] P. R. Rosenbaum. An exact distribution-free test comparing two multivariate distributions based on adjacency, *Journal of the Royal Statistical Society B*, 67:515–530, 2005.
- [16] Y. Saeys, I. Inza, P. Larrañaga, A review of feature selection techniques in bioinformatics. *Bioinformatics*, 23: 2507–2517, 2007.
- [17] J. A. Bibby, D. Agarwal D, T. Freiwald, N. Kunz, N.S. Merle, E. E. West, P. Singh, A. Larochelle, F. Chinian, S. Mukherjee, B. Afzali, C. Kemper and N. R. Zhang, Systematic single-cell pathway analysis to characterize early T cell activation, *Cell Reports*, 41(8):111697, 2022.
- [18] N. Smirnov, On the estimation of the discrepancy between empirical curves of distribution for two independent samples, *Bulletin de Universite de Moscow, Serie internationale (Mathematiques)*, Vol. 2, 3–14, 1939.
- [19] R. Tibshirani Regression shrinkage and selection via the lasso, *Journal of the Royal Statistical Society B*, 58:267–288, 1996.
- [20] A. Wald and J. Wolfowitz, On a test whether two samples are from the same population, *Annals of Mathematical Statistics*, 11(2):147–162, 06 1940.
- [21] L. Weiss, Two-sample tests for multivariate distributions, *The Annals of Mathematical Statistics*, Vol. 31, 159–164, 1960.
- [22] M.F. Schilling, Multivariate two-sample tests based on nearest neighbors, *Journal of the American Statistical Association*, Vol. 81, 799–806, 1986.
- [23] P. Cortez and A. Morais, A Data Mining Approach to Predict Forest Fires using Meteorological Data, *J. Neves, M. F. Santos and J. Machado Eds., New Trends in Artificial Intelligence, Proceedings of the 13th EPIA 2007 - Portuguese Conference on Artificial Intelligence*, 512–523, 2007.
- [24] S. Slovin, A. Carissimo, F. Panariello, A. Grimaldi, V. Bouché, G. Gambardella, D. Cacchiarelli, Single-Cell RNA Sequencing Analysis: A Step-by-Step Overview. *RNA Bioinformatics*, Springer US, New York, NY. 343–365, 2021.
- [25] K. Su, T. Yu and H. Wu, Accurate feature selection improves single-cell RNA-seq cell clustering, *Briefings in Bioinformatics*, ISSN. 1477–4054 (2), 2021.
- [26] F.W. Townes, S.C. Hicks, M.J. Aryee, R.A. Irizarry, Feature selection and dimension reduction for single-cell RNA-Seq based on a multinomial model, *Genome Biology*, Vol. 20, 295, 2019.
- [27] J.A. Shyer, R.A. Flavell and W. Bailis, Metabolic signaling in T cells, *Cell Research*, Vol. 30, 649–659, 2020.
- [28] N. Jones, J.G. Cronin, G. Dolton, S. Panetti, A.J. Schauenburg, S.A.E. Galloway, A.K. Sewell, D.K. Cole, C.A. Thornton, N.J. Francis, Metabolic Adaptation of Human CD4+ and CD8+ T-Cells to T-Cell Receptor-Mediated Stimulation, *Frontiers in Immunology*, Vol. 8, 1561, 2017.

- [29] A. M. Griesinger, D. K. Birks, A. M. Donson, V. Amani, L.M. Hoffman, A. Waziri, M. Wang, M. H. Handler and N. K. Foreman, Characterization of distinct immunophenotypes across pediatric brain tumor types. *Journal of Immunology*, 191(9), 4880-4888, 2013.
- [30] P. Langfelder, S. Horvath. WGCNA: an R package for weighted correlation network analysis. *BMC Bioinformatics*. 2008;9:559. doi: 10.1186/1471-2105-9-559.
- [31] BR. Zeeberg, W. Feng, G. Wang, et al. GoMiner: a resource for biological interpretation of genomic and proteomic data[J]. *Genome biology*, 2003, 4(4): R28.

EMAIL gswarnadip@gmail.com

EMAIL somabha@nus.edu.sg

EMAIL dagarwal@mgh.harvard.edu

EMAIL e0732876@u.nus.edu

EMAIL e0732845@u.nus.edu

EMAIL e0729791@u.nus.edu